Targeted gold nanorod contrast agent for prostate cancer detection by photoacoustic imaging

A. Agarwal
Department of Chemical Engineering, University of Michigan, Ann Arbor, Michigan 48109, USA

S. W. Huang and M. O'Donnell
Department of Biomedical Engineering, University of Michigan, Ann Arbor, Michigan 48109, USA

K. C. Day and M. Day
Department of Urology, University of Michigan, Ann Arbor, Michigan 48109, USA and Comprehensive Cancer Center, University of Michigan, Ann Arbor, Michigan 48109, USA

N. Kotov
Department of Chemical Engineering, University of Michigan, Ann Arbor, Michigan 48109, USA

S. Ashkenazi[a)]
Department of Biomedical Engineering, University of Michigan, Ann Arbor, Michigan 48109, USA

(Received 19 November 2006; accepted 2 August 2007; published online 19 September 2007)

A targeted gold nanoparticle has been developed as a contrast agent for photoacoustic medical imaging. We have studied cancer cell targeting by antibody conjugated gold nanorods for high contrast photoacoustic imaging. By changing the aspect ratio of the elongated "rod" shape of the gold nanoparticle, its plasmon peak absorption wavelength can be tuned to the near IR (700–900 nm) for an increased penetration depth into biological tissue. Effective cell targeting and sensitive photoacoustic detection of a single layer of cells are demonstrated. Combining ultrasound with contrast agent based photoacoustic imaging is proposed as a visual tool to compound molecular and structural information for early stage prostate cancer detection. © *2007 American Institute of Physics*. [DOI: 10.1063/1.2777127]

Optical absorption in metals is governed by plasmon excitation. In a metal nanoparticle, plasmon resonance leads to very highly efficient light absorption. Typically, the absorption cross section of a metal nanoparticle can be an order of magnitude larger than its geometrical cross-sectional area.[1] Its shape plays a crucial role in determining the peak absorption wavelength. For medical imaging applications, the resonance wavelength can be tuned within the "tissue transparent" window of 700–1000 nm to increase the penetration depth.

Several types of gold nanoparticles, such as nanospheres, nanoshells, and nanorods, have been shown to provide enhanced image contrast for optical imaging methods in medical applications.[2–4] Gold is preferred since it is biocompatible.[5,6] Functional and molecular properties can be imaged by targeting specific cells using antibody conjugated nanoparticles.

One of the most promising techniques for optical imaging in medical diagnostics is photoacoustics. The photoacoustic effect can be used to image the distribution of optical absorption in tissue. A short laser pulse illuminates the tissue, creating rapid heating and acoustic emission due to thermal expansion of tissue components. An ultrasonic array is used to detect the emitted acoustic field and reconstruct the initial heat distribution. The technique combines the specificity and sensitivity of optical imaging with the high resolution and penetration of ultrasound imaging.

Gold nanoparticles conjugated with an antibody have been used to enhance optical absorption (and photoacoustic signals) in targeted cancer tissue and provide high contrast for noninvasive cancer imaging.[7,8] In this work, we describe cancer cell targeting by gold nanorods conjugated with an antibody and demonstrate photoacoustic imaging of a single layer of cells. The specific nanoparticle complex described here was designed for peak absorption in the range of 700–840 nm, optimal for *in vivo* applications.

Gold nanorods were prepared using seed mediated growth,[9,10] a technique providing control over the size and aspect ratio. Particle size distribution was measured using transmission electron microscopy (TEM) imaging [see Fig. 1(a)]. The mean length is 45 nm and the mean diameter is 15 nm. The optical absorption of the sample was measured using a spectrophotometer (model 8453, Agilent, Santa

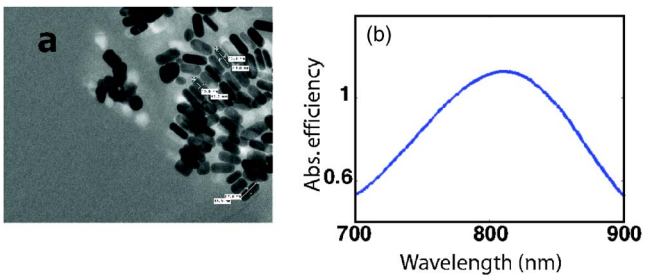

FIG. 1. (Color online) TEM image of a sample of gold nanorods (a) and optical absorption efficiency (single particle absorption cross section normalized by its geometrical cross-sectional area) of the sample (b).

[a)]Electronic mail: shaia@umich.edu

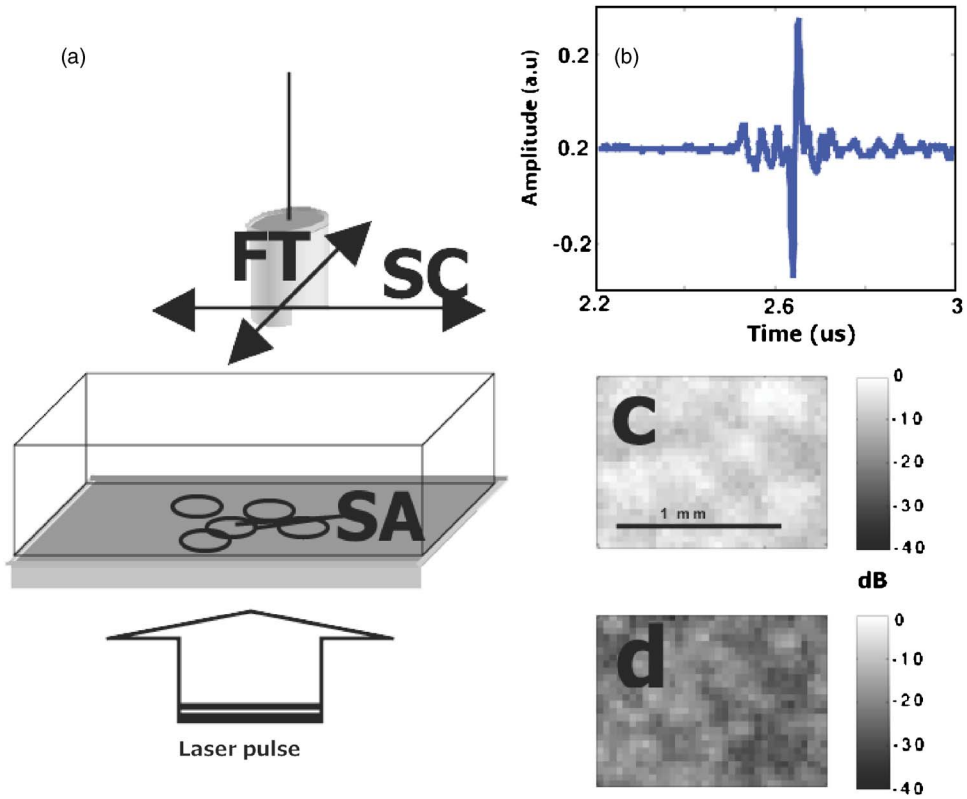

FIG. 2. (Color online) High frequency photoacoustic two-dimensional (2D) scanning device. Pulsed laser illuminates a sample (SA) from the bottom. An *XY* motorized stage (SC) scans a focused ultrasound transducer (FT) with its focal plane aligned to the sample bottom (a). Transducer signal from a single layer of cells targeted by antibody conjugated gold nanorods (b). High resolution scan of photoacoustic signal of LNCaP cells incubated with antibody conjugated gold nanorods (c) and with bare gold nanorods (d) at an illumination wavelength of 706 nm.

Clara, CA). The absorption peak is at 810 nm. The absorption efficiency, defined as the ratio of the single particle absorption cross-section to its geometrical cross-sectional area (45×15 nm^2), is shown in Fig. 1(b). Other samples with peak absorption in the range of 700–840 nm were prepared for imaging experiments.

We chose a LNCaP prostate cancer lines[11,12] as target cells for this study. This cell line was derived from lymph node metastasis of prostate cancer and is widely used as a disease model. These cells overexpress the transmembrane receptor Her-2/neu.[13] A monoclonal antibody (Ab-17, Lab Vision), designed specifically for the Her-2/neu antigen, was targeted to these cells. Synthesized gold nanorods have a bilayer of a positively charged surfactant hexadecyltrimethylammonium bromide (CTAB) which acts as a stabilizer to prevent aggregation. A layer of polyacrylic acid (PAA) is adsorbed on the surface to obtain a–COOH functional group used to conjugate the antibody.

LNCaP cells were grown on a double compartment cell culture chamber (CultureSlides, BD Falcon™, and BD BioCoat™). They form a single layer on the dish bottom. Cell mean size and density were measured by optical microscopy to be 15 ± 4 μm and 230 ± 30 cells/mm^2, respectively. The first compartment was filled with antibody conjugated gold nanorods suspended in phosphate buffer saline (PBS). The second compartment was filled with gold nanorods suspended in PBS with no antibody conjugation. This compartment served as a control to estimate the level of nonspecific binding to the cells. Both compartments were incubated at room temperature for 1 h using an identical nanoparticle concentration of 10^{12} particles/ml. After incubation, the container was washed three times with PBS and then placed in the sample holder of the photoacoustic scanning setup described in Fig. 2(a).

A pulsed doubled neodymium-doped yttrium aluminum garnget (Nd:YAG) laser (Surelite I-20, Continuum, Santa Clara, CA) is used to pump an optical parametric oscillator (OPO) (Surelite OPO PLUS, Continuum) which emits 5 ns pulses, with 12 mJ pulse energy and tunable wavelength in the range of 690–980 nm. The laser beam is first expanded to a diameter of 20 mm and then directed to illuminate the sample bottom. A focused ultrasonic transducer ($LiNbO_3$, 50 MHz, and $f/1.5$) is used to detect the photoacoustic signal. The focal plane of the transducer is aligned with the bottom of the cell culture chamber. A motorized *XY* stage is used to scan the transducer across the sample to map the photoacoustic signal. The resolution of the scan is limited by the spot size of the transducer at the focal plane (50 μm). The transducer output is amplified (model 5910PR, Panametrics) and digitized by a digital oscilloscope (WaveSurfer 432, LeCroy Corp. Chestnut Ridge, NY).

Scans of the two compartments are given in Figs 2(c) and 2(d) for an illumination wavelength of 706 nm (matching peak absorption of the gold nanorod sample used). The signal in the first compartment is higher by 20 dB than that in the second (control), indicating an order of magnitude higher nanoparticle concentration due to specific binding of the antibody to the antigen. The lower signal in the control compartment is attributed to nonspecific binding to the cell layer due to surface charge interactions. The cell density in the sample corresponds to less than one cell (~0.5 cell in a 50 μm diameter circular area) in the active detection area of the transducer. Therefore, the detected signal is primarily contributed by the acoustic emission from a single cell. The

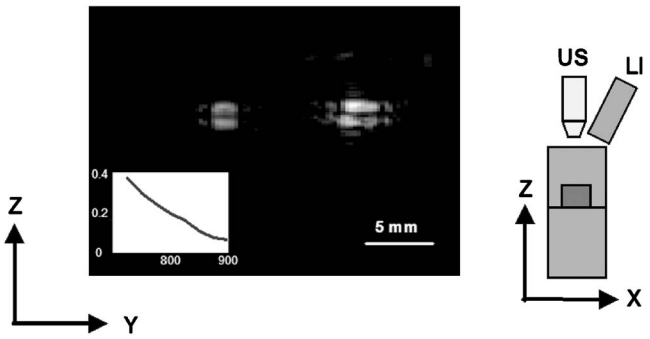

FIG. 3. (Left) Photoacoustic image of a phantom object at illumination wavelength of 725 nm with two different concentrations of gold nanorods: 6.5×10^{11} (right) and 2.6×10^{10} (left) nanoparticles/ml. (Right) Imaging setup including the fiber bundle line illuminator (IL), the ultrasound probe (US), and the phantom object.

signal detected from the targeted monolayer of cells is shown in Fig. 2(b).

Based on these initial studies, we have explored whether a more clinically relevant photoacoustic imaging system can detect targeted nanoparticles at similar concentrations. For prostate cancer detection, a more practical approach would use a transrectal ultrasound (TRUS) imaging probe to detect the photoacoustic emission while providing laser pulse illumination through fiber optic light guides. To implement this design concept, we have constructed a photoacoustic imaging system composed of a commercial ultrasound scanner (Sonix RP, Ultrasonix, Burnaby, BC, Canada) synchronized with the pulsed doubled YAG laser pumped OPO described earlier. For preliminary *in vitro* and small animal experiments we have equipped the system with a 10 MHz linear array probe (L14-5/38, Ultrasonix). Dedicated operating software was written to acquire rf signals from each element in the array in synchronization with the laser pulse. A beam forming algorithm was implemented for image reconstruction.[14–16]

A phantom object was constructed to test the detection limit as a function of particle concentration. The phantom consists of two inclusions of gelled nanoparticle suspension embedded in a mixture of agarose gel (GPG/LE, American Bioanalytical) and 5% Intralipid (Liposyn® II 10%, Abbott Laboratories). The inclusions have a rectangular prism shape of 1×3 mm^2 cross section. The nanoparticle concentrations in the two inclusions are 6.5×10^{11} and 2.6×10^{10} particles/ml. To acquire photoacoustic images the phantom was illuminated from above (see Fig. 3) using a fiber bundle line illuminator (Edmunds Optics, #57019) coupled to the pulsed Nd:YAG laser (pulse energy of 30 mJ, spot size of 16×40 mm^2, and light fluence of 4.6 mJ/cm^2). A series of images was acquired using different wavelengths in the range of 725–900 nm. To reduce noise signals were averaged 16 times. Figure 3 shows a photoacoustic image acquired at 725 nm which corresponds to the peak absorption of the gold nanorod sample used in this experiment. The inset shows the relative photoacoustic energy detected from the high concentration object at different wavelengths. The detection level of the lower concentration object is 10 dB above the noise. The absorption coefficient at the lower concentration is 0.2 cm^{-1}.

In a recent measurement of optical properties of human prostate,[17] a mean value of 0.23 cm^{-1} was obtained for the tissue absorption coefficient, with interpatient variation of 0.13 cm^{-1}. To detect gold nanorods in tissue with sufficient contrast, the optical absorption should be at least five times higher than the tissue background. This corresponds to a gold nanorod concentration of about 1.5×10^{11} particles/ml. Based on the phantom measurement, conducted using light fluence four times below ANSI Z136 safety limit (20 mJ/cm^2), we conclude that at this concentration, image contrast ratio of 5 would be achieved with instrumental noise well below the tissue background.

Nanoparticle based contrast enhancement was also demonstrated for magnetic resonance imaging (MRI).[18] The

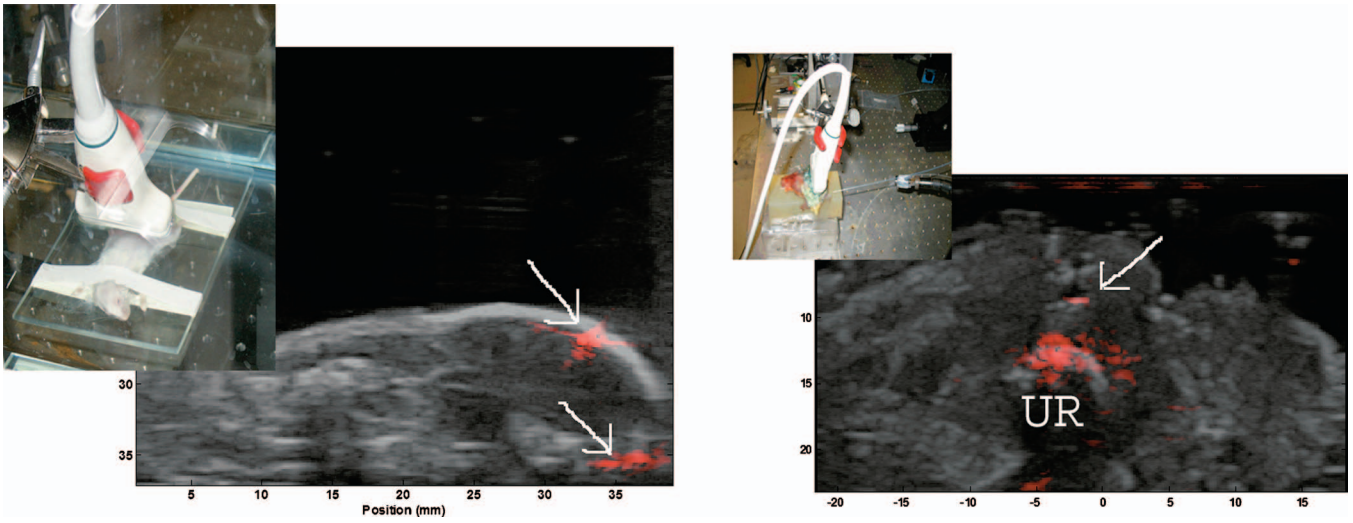

FIG. 4. (Color) (Left) A combined US/PA image of a mouse hind limb with two gold nanorod gelled inclusions implanted in its right hip. Arrows show the locations of implanted gelled nanorod solution. (Left inset) The mouse was fixed in a water tank with the ultrasonic transducer positioned above its lower body. (Right) Combined US/PA image of human prostate gland with a gold nanoparticle sample implanted in an incision made on it's top part (marked by arrow). (Right inset) Imaging setup including the ultrasound probe and fiber illumination inserted through the urethra (UR).

minimal particle concentration required for detecting 0.5 mm objects using gadolinium-perfluorocarbon particles (250 nm in size) was assessed to be 0.6×10^{11} particles/ml. This value is comparable to the minimal concentration required for gold nanorod enhanced photoacoustic imaging, while the particle size used in MRI is almost an order of magnitude larger.

A major advantage of using an ultrasound scanner to acquire photoacoustic images is the simplicity of combining conventional ultrasound with photoacoustic imaging. Since the same probe is used for both, coregistration is straightforward and accurate. To demonstrate the effectiveness of a combined ultrasound/photoacoustic (US/PA) image, we have performed two imaging experiments. In the first experiment, we have implanted two small objects made of gelled nanoparticle solution (1.5 mm diameter cylinders of 4 and 2 mm lengths and nanorod concentration is 6×10^{11} nanoparticles/ml) in the upper part of a mouse hind limb. The probe was positioned to image a transverse cross section of the mouse hind limbs. A laser beam (12 mJ and 25 mm diameter) was directed to illuminate the implanted location. Ultrasound and photoacoustic images were acquired at the same position and combined later using different color maps for ultrasound (gray scale) and photoacoustic (red) images. The combined image is presented in Fig. 4(a), clearly showing the two inclusions. In a second experiment, we have implanted a small (1 mm size cube and nanorod concentration is 6×10^{11} nanoparticles/ml) nanoparticle gel object into an incision made in a cadaver human prostate gland. The prostate was illuminated by a fiber (1 mm core diameter) inserted through the urethra. The pulse energy emitted from the tip of the fiber is 1.5 mJ. The combined image [Fig. 4(b)] clearly shows the incision and the nanoparticle object. Photoacoustic signal is also observed in the region of the urethra. This artifact is caused by the high optical fluence near the fiber tip and could be reduced by properly designed optical diffuser.

In conclusion, multimodality imaging for cancer detection is introduced. The image is composed of an ultrasonic pulse-echo image and a photoacoustic image based on a targeted gold nanorod contrast agent. We have demonstrated that gold nanorods produce high contrast between targeted tissue and nontargeted tissue for photoacoustic imaging in an *in vitro* experiment. Combining high contrast and cell specific targeting with ultrasonic structural imaging would provide a clear anatomical view with targeted tissue highlighted in a contrasting color. This technique is highly attractive for early detection of prostate cancer. Using a TRUS probe equipped with fiber optic illumination, the physician can image tissue structure and diagnose lesions by their cell type, avoiding unnecessary biopsy procedures. In cases where biopsy is administered, tissue sampling accuracy can be improved with image guidance. It can be applied to the detection of other lesions, such as breast, bladder, and ovarian cancers, by applying a suitable ultrasound probe and light delivery device. Other clinical applications can be developed based on similar principles to image specific molecular and functional information by targeting cell expression of various transmembrane receptors.

[1] P. K. Jain, K. S. Lee, I. H. El-Sayed, and M. A. El-Sayed, J. Phys. Chem. B **110**, 7238 (2006).
[2] I. H. El-Sayed, X. Huang, and M. A. El-Sayed, Nano Lett. **5**, 829 (2005).
[3] C. Loo, A. Lowery, N. Halas, J. West, and R. Drezek, Nano Lett. **5**, 709 (2005).
[4] K. Sokolov, M. Follen, J. Aaron, I. Pavlova, A. Malpica, R. Lotan, and R. Richards-Kortum, Cancer Res. **63**, 1999 (2003).
[5] E. E. Connor, J. Mwamuka, A. Gole, C. J. Murphy, and M. D. Wyatt, Small **1**, 325 (2005).
[6] C. M. Goodman, C. D. McCusker, T. Yilmaz, and V. M. Rotello, Bioconjugate Chem. **15**, 897 (2004).
[7] A. Conjusteau *et al.*, Proc. SPIE **60860**, 60860K (2006).
[8] P.-C. Li, C.-W. Wei, C.-K. Liao, C.-D. Chen, K.-C. Pao, C.-R. C. Wang, Y.-N. Wu, and D.-B. Shieh, Proc. SPIE **6086**, 60860M (2006).
[9] B. Nikoobakht and M. A. El-Sayed, Chem. Mater. **15**, 1957 (2003).
[10] J. H. Song, F. Kim, D. Kim, and P. Yang, Chem.-Eur. J. **11**, 910 (2005).
[11] M. E. Stearns *et al.*, Prostate **36**, 56 (1998).
[12] N. Sato, M. E. Gleave, N. Bruchovsky, P. S. Rennie, E. Beraldi, and L. D. Sullivan, Cancer Res. **57**, 1584 (1997).
[13] D. B. Agus, H. I. Scher, B. Higgins, W. D. Fox, G. Heller, M. Fazzari, C. Cordon-Cardo, and D. W. Golde, Cancer Res. **59**, 4761 (1999).
[14] M. Xu and L. V. Wang, IEEE Trans. Med. Imaging **21** (2002).
[15] R. A. Kruger, P. Y. Liu, Y. R. Fang, and C. R. Appledorn, Med. Phys. **22**, 1605 (1995).
[16] V. A. Andreev, A. A. Karabutov, S. V. Solomatin, E. V. Savateeva, V. Aleynikov, Y. V. Zhulina, R. D. Fleming, and A. A. Oraevsky, Proc. SPIE **3916**, 36 (2000).
[17] T. C. Zhu *et al.*, Photochem. Photobiol. **81**, p. 96 (2005).
[18] A. M. Morawski *et al.*, Magn. Reson. Med. **51**, 480 (2004).